

# TTA-Nav: Test-time Adaptive Reconstruction for Point-Goal Navigation under Visual Corruptions

Maytus Piriyaajakonkij<sup>1</sup>, Mingfei Sun<sup>1</sup>, Mengmi Zhang<sup>2,3</sup>, and Wei Pan<sup>1</sup>

**Abstract**—Robot navigation under visual corruptions presents a formidable challenge. To address this, we propose a Test-time Adaptation (TTA) method, named as TTA-Nav, for point-goal navigation under visual corruptions. Our “plug-and-play” method incorporates a top-down decoder to a pre-trained navigation model. Firstly, the pre-trained navigation model receives a corrupted image input and extracts features. Secondly, the top-down decoder produces the reconstruction given the high-level features extracted by the pre-trained model. Then, the decoder feeds the reconstruction of a corrupted image back to the pre-trained model, which outputs the final action. Despite being trained solely on clean images, the top-down decoder reconstructs cleaner images from corrupted ones without gradient-based adaptation. The pre-trained navigation model with our top-down decoder significantly enhances navigation performance across almost all visual corruptions in our benchmarks. Our method improves the success rate of point-goal navigation from the state-of-the-art result of 46% to 94% on the most severe corruption, showing the potential for broader application in robotic visual navigation. Project page: <https://sites.google.com/view/tta-nav>

## I. INTRODUCTION

Robot navigation faces substantial challenges when confronted with visual corruptions [1], [2], [3], [4], [5], as illustrated in Fig. 1: The robot is equipped with a state-of-the-art (SOTA) navigation model trained on 2.5 billion clean frames with deep reinforcement learning (DRL). Despite being trained on a great amount of data, the robot still fails to navigate to the target position under dimmed lighting. Unforeseeable visual corruptions can occur during the test time and these corruptions are harmful to navigation performance.

This challenge raises questions about the adaptability of robots: How can a robot dynamically adjust in real-time to visual corruptions that are unforeseeable in the training phase? And how can it maintain effective navigation when encountering such corruption despite being trained solely on clean observations? The previous work [5] considers the navigation with a map, which can be deteriorated if the camera images are corrupted, and proposes a map refiner to generate a more precise map. However, their method requires the robot to collect data and gradient-based fine-tuning in the test time. That means the robot has a distinct fine-tuning and test phase. This is impractical in some applications that

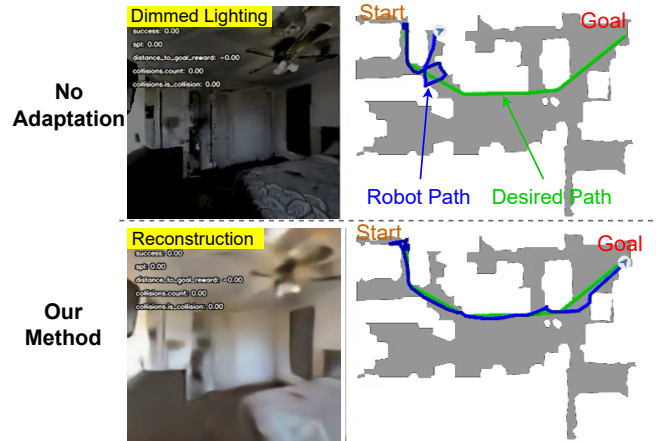


Fig. 1. **Point-Goal Navigation Under Visual Corruptions:** A robot is tasked to move from start to goal position. *Top:* The robot is equipped with the state-of-the-art navigation method [6]. It fails to navigate from the bedroom to another room when facing the dimmed light condition. *Bottom:* The robot is equipped with our method. It receives the reconstructed image as the “surrogate observation” instead of the real observation from the scene.

require the robot to immediately adapt to corruption, such as self-driving cars.

To this end, we propose a Test-time Adaptation (TTA) method for robot navigation under visual corruptions. Our method is inspired by the top-down processing observed in human cognition [8]. This processing is deemed as a fundamental mechanism for solving challenging visual tasks [9], [10]. Specifically, consider a Deep Neural Network (DNN) model as an architecture with low-level visual processing at earlier layers and high-level visual processing at later layers, our method relies on top-down modulation from a decoder, which receives the high-level features of an image extracted by the pre-trained visual perception model, reconstructs the clean observation and feeds reconstructed inputs back to the visual perception model. The other key mechanism of our method is adaptive normalization (AN) in the pre-trained visual perception model. During the test phase, AN adjusts normalization statistics via a moving average update, denoises image features, and enables the decoder to reconstruct cleaner images. Our method enables the robot to navigate using these reconstructed images as surrogate observations instead of the actual observations. The decoder is trained via self-supervised learning on “uncorrupted” images to learn a representation capable of reconstructing input images. Interestingly, the decoder can reconstruct cleaner images given corrupted images during the test phase.

In summary, we develop a benchmark consisting of 13 types of visual corruptions to evaluate how navigation per-

<sup>1</sup> Department of Computer Science, The University of Manchester, Manchester, United Kingdom.

<sup>2</sup> Centre For Frontier AI Research, Agency for Science, Technology and Research (A\*STAR), Singapore.

<sup>3</sup> School of Computer Science and Engineering, Nanyang Technological University, Singapore.

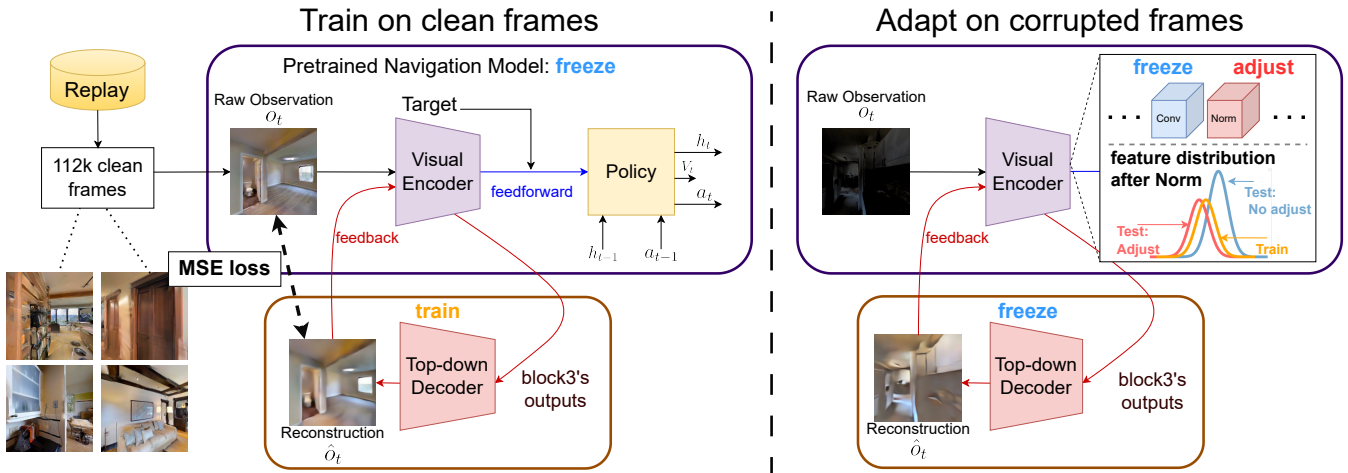


Fig. 2. **An overview of our proposed method (TTA-Nav):** We present the pretrained navigation model (Pretrained-Nav), which contains Visual Encoder (VE) and policy network, in the purple frame. TTA-Nav is a plug-and-play method. It has Top-down Decoder (TD) in the orange frame. TD receives the output of the late layer of VE and projects the reconstructed image back to the VE’s input layer. Here, VE is SE-ResNeXt-50 [7] and TD receives block3’s output. **Left:** During training, VE remains fixed, while TD is trained to predict VE’s input by minimizing Mean Squared Error (MSE) loss. Training occurs offline, utilizing samples from Replay, which contains the visual experiences of a robot navigating 72 Gibson training scenes. **Right:** During testing, TD is frozen and the BatchNorm layers of VE can adjust their normalization statistics  $\hat{\mu}_k$  and  $\hat{\sigma}_k$ . See section III for more details. Finally, the reconstructed image is input to VE for navigation. VE does feedforward computation again and the policy outputs actions.

formance degrades under each corruption type, as detailed in Fig. 3. These challenges highlight the limitations of non-adaptive models in maintaining effective navigation under visual corruptions. Here, “non-adaptive” refers to models that do not dynamically adjust their processing or decision-making mechanisms in response to changes in visual input quality. Then, we propose a TTA method for point-goal navigation, named TTA-Nav, which can be seamlessly integrated, i.e., “plug-and-play”, into existing navigation models without re-training. Particularly, TTA-Nav leverages adaptive normalization in the pre-trained visual perception model to denoise image features, and uses a top-down decoder to reconstruct cleaner versions of corrupted images from the high-level features. Our method improves navigation performance without explicitly fine-tuning the decoder on corrupted inputs. It outperforms three state-of-the-art TTA methods: DUA [11], TENT [12], and SHOT-IM [13]. This is evidenced across our visual corruption benchmarks, where TTA-Nav consistently shows improved performance.

## II. RELATED WORK

### A. Visual Navigation

Robotic navigation has a long historical background, initially relying on classical methods centered around planning on constructed maps [14], [15], necessitating localization and mapping techniques [16]. With the advent of deep learning, there has been a shift towards end-to-end models [17] that directly translate observations into actions. These models are typically trained using Deep Reinforcement Learning (DRL) [18], [17] and/or Imitation Learning [19]. Navigation tasks often involve various types of goals, such as point goals [20], [6] (moving to a specified position), object goals [21], [22] (reaching a position where a specific object is located), image goals [23] (navigating to a position corresponding to a target image), and language goals [24] (following verbal commands). Despite their differing objectives, these goals

share the common structure of moving from one location to another. Notably, certain navigation tasks, like object-goal navigation, can be accomplished using point-goal agents without additional training [25]. While point-goal navigation achieves near-perfect performance under ideal conditions of precise odometry and clear observations [6], the performance may significantly decline in the presence of visual corruptions [1], [3], [4], [2]. This comes to interest and contribution of our study.

### B. Domain Generalization (DG)

DG addresses a scenario wherein a model is tasked with learning representations that can generalize across unseen input distributions, while facing identical tasks as during training. To solve DG problems, data augmentation techniques are the most common. It is implemented by introducing random variations or perturbations to the training environment’s parameters, such as textures, lighting, or physics, to create a diverse set of training scenarios [26], [27]. During testing, the learned weights and biases remain fixed, thereby preventing agents from leveraging test data to adjust parameters. In contrast, our approach advocates for the utilization of a test data stream to dynamically adjust model parameters in real time.

### C. Domain adaptation (DA)

DA entails adapting a model trained on the data from the source domain to the data from the target domain, notwithstanding variations in distribution, characteristics, and other factors between the two domains. Unlike DG, unsupervised DA operates under the assumption that some portion of test data is accessible [28], [29] (e.g., unlabeled test images). In these studies [30], [5], researchers propose methods for refining a generated map of an unseen scene with noisy actuator and dynamic, visual corruptions. Subsequently, the navigation model utilizes this refined map to make decisions. In contrast to our approach, their models rely on map-based

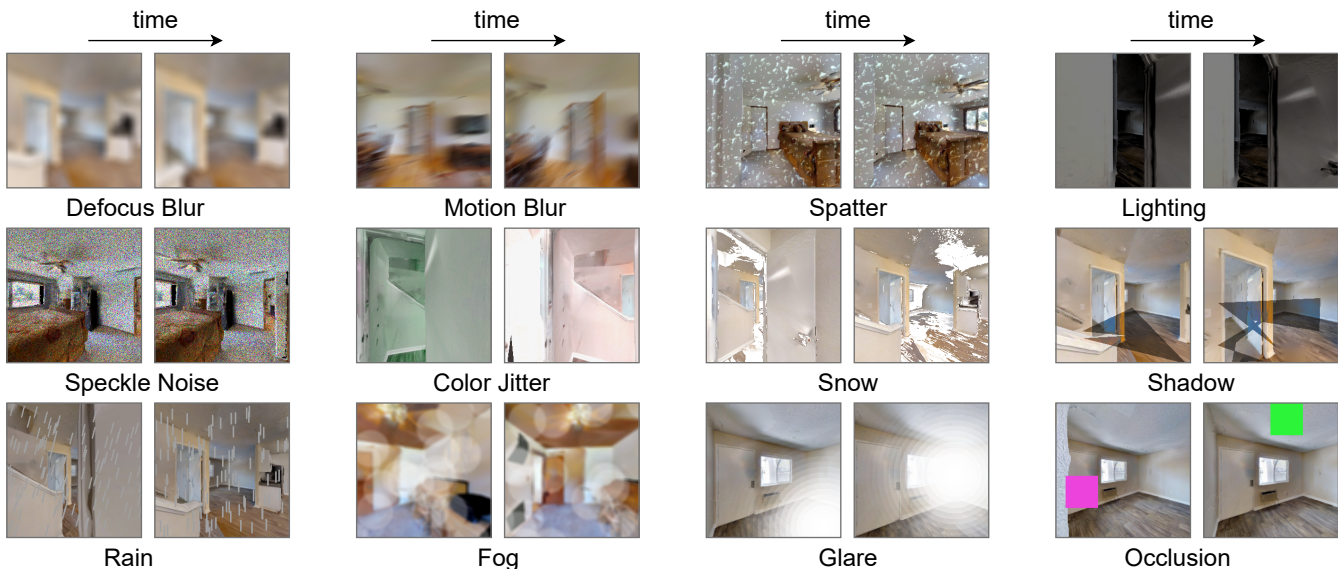


Fig. 3. **Visual Corruptions:** Two consecutive images of the same corruption type are in temporal order, as indicated by the arrow. Every corruption is induced frame by frame, so the corruption in the frame  $t$  is independent to the corruption in the frame  $t + 1$ . For instance, at the bottom right, the position and color of a box at the time  $t$  is independent to the position and color of a box at the time  $t + 1$  in Occlusion type.

policies and undergo a fine-tuning phase using test data. Our method, on the other hand, is an end-to-end DRL model that learns to directly map raw observations to actions. Notably, our adaptation process operates in real time and requires no fine-tuning on test data.

#### D. Test-time adaptation (TTA)

Unlike DA, TTA model does not have access to samples or information about the specific distribution of the test data it will encounter during inference [31], [12], [13], [32], [11], [33]. TTA enables the model to adjust its predictions dynamically based on the characteristics of the test data it sees during inference. This adaptation can occur in real time as the model encounters new examples, allowing it to continually refine its performance based on the incoming data stream. TTA methods improve the model’s accuracy on multiple classification tasks when models face visual corruptions such as image recognition [12], [13], [34], object detection [11], semantic segmentation [35] and video recognition [33]. Most of the SOTA methods are task-specific [35], [36], [37], [38], [33], and TTA method for DRL is under-explored. We investigate three methods (DUA [11], TENT [12], and SHOT-IM [13]) because they are task-agnostic and can be seamlessly integrated into a general DRL model. Subsequently, we introduce TTA-Nav, which surpasses the performance of all aforementioned approaches.

### III. METHODS

In this section, we will present technical details of the proposed TTA method for point-goal navigation under visual corruption. We will first review the formulation of the point-goal navigation problem. Then, we will describe the existing navigation models that will be used in our experiments. To conclude this section, we present the algorithm of our proposed method.

#### A. Point-Goal Navigation Problem Formulation

In point-goal navigation, a robot is tasked to move to the given relative direction:  $(\Delta x_{\text{target}}, \Delta y_{\text{target}}) = (x_{\text{target}} - x_{\text{start}}, y_{\text{target}} - y_{\text{start}})$  in a cluttered indoor scene. For instance, given the goal of moving to  $(\Delta x_{\text{target}} = 0.5m, \Delta y_{\text{target}} = -2m)$ , the robot has to move to the target position  $(x_{\text{start}} + 0.5, y_{\text{start}} - 2)$ , where  $(x_{\text{start}}, y_{\text{start}})$  is the initial position. The short path will lead to the high reward given to the robot. In our setting, the robot is equipped with a navigation model trained with clean RGB observations and GPS & Compass  $(x_{\text{target}} - x_t, y_{\text{target}} - y_t)$ . The GPS & Compass is derived from the error-free odometry  $(\Delta x_t, \Delta y_t)$ . Where  $\Delta x_t = x_t - x_{t-1}$ ,  $\Delta y_t = y_t - y_{t-1}$ , and  $(x_t, y_t)$  is the position of the robot at time  $t$ . The robot can take 4 actions: move forward (0.25m), turn left ( $10^\circ$ ), turn right ( $10^\circ$ ) and stop. Once the robot takes stop action, an episode will end. During the evaluation, we allow the robot to take up to 500 environment steps in an episode, i.e., timed-out steps. We use the Gibson scene dataset [39] by following the standard train and validation split as in [23] which yields 72 training and 14 validation scenes. The robot is trained with training scenes and evaluated with 14 unseen validation scenes (994 episodes). We use Habitat platform [20], [40], [41] as an environment.

#### B. End-to-End Visual Navigation Models

Generally, an end-to-end visual navigation model can be decomposed into two parts: Visual Encoder (VE) and a policy network. VE gets an RGB observation and extracts useful features for the task. Then, the policy network is given the target destination and uses the extracted features along with the target location to output action [17]. The models can be trained with reinforcement (RL) and/or imitation learning (IL) [19]. The overview architecture of the navigation models we used is in the purple frame in Fig. 2. In our study, we adopt the SOTA navigation model from [6]. It is trained with 2.5 billion RGB frames on a point-goal navigation task.

These RGB frames are obtained from both Gibson 2+ dataset (train) [39] and Matterport3D dataset (train and validation) [42]. We will call this model DD-PPO in the remaining parts of the text.

Our algorithm is based on the batch normalization (Batch-Norm) [43] but the pretrained DD-PPO model has group normalization (GroupNorm) [44]. Therefore, we replace all GroupNorm layers with BatchNorm and fine-tune the model on Gibson scenes for 120M frames using the same configurations as in [6]. Specifically, we adopt SE-ResNeXt-50 [7] for VE architecture and LSTM [45] with the hidden size of 512 for the policy network. We use the same reward function as proposed in [6]. We will call this model as Pretrained-Nav.

### C. Algorithm

---

#### Algorithm 1 TTA-Nav: Training

---

```

1: VE is denoted as  $f_\phi$ . TD is denoted as  $g_\theta$ 
2:  $f_\phi^{b_3}(\cdot)$  returns VE block3's output
3: freeze  $f_\phi$ 
4: while not converge do
5:    $o = \text{sample}(\text{Dataset})$            ▷ batch of observations
6:    $z = f_\phi^{b_3}(o)$                    ▷ get block3's output
7:    $\hat{o} = g_\theta(z)$                    ▷ reconstruction
8:    $\mathbf{L}_{mse}(\theta) = \sum_i (o_i - \hat{o}_i)^2$    ▷ calculate loss
9:    $\theta = \text{update}(\theta, \mathbf{L}_{mse}(\theta))$    ▷ update by ADAM
10: end while

```

---



---

#### Algorithm 2 TTA-Nav: Adaptation

---

```

1: policy is denoted as  $\pi_\phi$ 
2:  $h_t$  is the hidden state of LSTM
3:  $\mu_k, \sigma_k$  in  $f_\phi$  to be updated as in (2) and (3)
4: for every time step  $t$  do
5:   Get  $o_t$  from the environment
6:    $z_t = f_\phi^{b_3}(o_t)$                  ▷ get block3's output
7:    $\hat{o}_t = g_\theta(z_t)$                  ▷ reconstruction
8:    $e_t = f_\phi(\hat{o}_t)$                  ▷ VE gets reconstructed input
9:    $a_t = \pi_\phi(e_t, h_{t-1}, \text{target})$  ▷ policy returns action
10: end for

```

---

We now introduce TTA-Nav, a plug-and-play method that can be added to Pretrained-Nav and requires no modification of the main model. TTA-Nav introduces Top-down Decoder (TD) denoted as  $g_\theta$  that receives the output of the late layer of VE and predicts the reconstructed image  $\hat{o}_t$ . See Fig. 2. TD comprises residual block modules adapted from architectures proposed in [46], [47]. This decoder produces RGB images with dimensions of  $256 \times 256$ . It has 5.3M trainable parameters.

**Training:** During the training of TTA-Nav, we freeze all VE parameters and train TD with mean squared error (MSE) reconstruction loss with samples from 72 training scenes of Gibson [39] without visual corruption. TD is trained with a very small subset of navigation data: 112k out of 2.5 billion frames. We follow the same optimization hyperparameters as in [47]. Specifically, we use ADAM optimizer [48] with the

learning rate of  $2 \times 10^5$ , and the momentum of 0.9999. See Algorithm 1 for more details.

**Adaptation:** TTA-Nav allows batch statistics in the Batch-Norm layers of the VE to be updated during the test time. We call this test-time update adaptive normalization. Specifically, each batch normalization layer normalizes an incoming sample  $x$  by the estimated mean and variance as in (1),

$$\hat{x} = \frac{x - \hat{\mu}_k}{\hat{\sigma}_k} \cdot \beta + \gamma, \quad (1)$$

where  $\beta$  and  $\gamma$  are affine parameters that scale and shift the data distribution respectively. Instead of estimating the mean and variance by averaging samples in a batch, we set VE to update the mean and variance by the moving average equations as in (2) and (3) below,

$$\hat{\mu}_k = (1 - \rho) \cdot \hat{\mu}_{k-1} + \rho \cdot \mu_k, \quad (2)$$

$$\hat{\sigma}_k^2 = (1 - \rho) \cdot \hat{\sigma}_{k-1}^2 + \rho \cdot \sigma_k^2, \quad (3)$$

where  $\hat{\mu}_k$  is the estimated mean and  $\hat{\sigma}_k^2$  is the estimated variance,  $\mu_k$  and  $\sigma_k^2$  are the sample mean and variance of the batch data, and  $\rho$  is a hyperparameter called momentum, which determines the contribution of the most recent sample estimate ( $\mu_k, \sigma_k^2$ ) to the calculation of the average. Here we update  $\mu_k$  and  $\sigma_k$  at every environment step, so the batch size is 1. See Algorithm 2 for more detail. In subsection IV-D, we will show that this simple adaptation can restore clean images from visual corruption.

## IV. EXPERIMENTS

We will describe the experimental setup which includes visual corruptions, baseline methods, and evaluation metrics. Subsequently, we will show experimental results in the following sequence. Firstly, we examine the visual content reconstructed by TD to illustrate why TTA-Nav is effective for navigation under visual corruptions. Secondly, we compare TTA-Nav with the baseline methods on clean and corrupted observations. Lastly, we conduct an ablation study to see what components lead to improvement in performance. All models in all experiments are first trained on clean observations and then adapt to changing environments with different corruptions during the testing phase.

### A. Visual Corruptions

The implementations of *Defocus Blur*, *Motion Blur*, *Lighting*, *Spatter*, and *Speckle Noise* are from the Habitat robustness benchmark dataset [3]. The implementations of weather corruptions (*Snow*, *Rain*, *Fog*, *Glare*, and *Shadow*) are from Alumentations [49]. The rest corruption types are implemented in the following ways: *Light Out* is implemented by filling the entire frames with zeros with an 85% probability, for example, if we sample 100 frames we will be likely to have around 85 black frames. *Color Jitter* is implemented by randomly adjusting the brightness, contrast, saturation, and hue of a frame. *Occlusion* is implemented by adding a  $64 \times 64$  box at a random position with a random color in a frame. See Fig. 3 for the example visualization of all corruption types.



Fig. 4. **Reconstructions from Top-down Decoder (TD)**: The left columns are the inputs of Visual Encoder (VE). *No Adapt*: Images in this column are the reconstructions from VE’s inputs without adaptation. *Adapt*: Images in this column are reconstructions from the same VE’s inputs with adaptation. The quality of reconstructed images matters in navigation. For example, bad reconstructions, shown in row 12 (Fog) and row 13 (Shadow) in Table I, may degrade navigation performance compared to non-adaptive approaches.

TABLE I

**NAVIGATION PERFORMANCE OF AGENTS WITH DIFFERENT ADAPTATION METHODS**: \* INDICATES CORRUPTION TYPES THAT CAUSE SEVERE DEGRADATION IN THE PERFORMANCE OF DD-PPO. **BOLD** INDICATES THE BEST SCORE AND **BROWN** INDICATES THE SECOND BEST SCORE AMONG OTHERS IN THE SAME ROW.

Corruption Type ↓	TENT		TENT-DUA		SHOT-IM		DD-PPO		Pretrained-Nav		DUA		TTA-Nav (Ours)	
	SR	SPL	SR	SPL	SR	SPL	SR	SPL	SR	SPL	SR	SPL	SR	SPL
Clean	0.52	0.45	0.96	0.86	0.90	0.82	<b>0.98</b>	<b>0.91</b>	<b>0.97</b>	<b>0.88</b>	0.94	0.83	<b>0.97</b>	0.86
Speckle Noise*	0.22	0.18	0.86	0.77	0.81	0.72	0.46	0.30	0.67	0.41	<b>0.92</b>	<b>0.77</b>	<b>0.94</b>	<b>0.81</b>
Lighting*	0.14	0.11	0.29	0.25	0.32	0.27	0.51	0.30	0.69	0.44	<b>0.87</b>	<b>0.68</b>	<b>0.91</b>	<b>0.78</b>
Spatte*	0.20	0.16	0.58	0.51	0.53	0.46	0.60	0.41	0.71	0.46	<b>0.89</b>	<b>0.74</b>	<b>0.95</b>	<b>0.84</b>
Rain*	0.17	0.14	0.28	0.24	0.30	0.25	0.75	0.53	0.78	0.56	<b>0.87</b>	<b>0.71</b>	<b>0.93</b>	<b>0.81</b>
Defocus Blur*	0.17	0.13	0.27	0.23	0.46	0.39	0.70	0.56	0.76	0.55	<b>0.87</b>	<b>0.71</b>	<b>0.85</b>	<b>0.67</b>
Snow	0.24	0.19	0.29	0.24	0.42	0.35	0.86	<b>0.70</b>	0.81	0.59	<b>0.87</b>	<b>0.69</b>	<b>0.88</b>	<b>0.69</b>
Motion BLur	0.20	0.16	0.30	0.26	0.79	0.70	0.83	<b>0.71</b>	0.82	0.64	<b>0.88</b>	<b>0.72</b>	<b>0.86</b>	0.70
Color Jitter	0.28	0.24	0.33	0.28	0.47	0.41	0.89	0.77	0.81	0.61	<b>0.90</b>	<b>0.78</b>	<b>0.94</b>	<b>0.83</b>
Glare	0.15	0.12	0.30	0.26	0.28	0.24	<b>0.90</b>	<b>0.79</b>	<b>0.89</b>	<b>0.74</b>	0.87	0.72	<b>0.89</b>	0.73
Light Out	0.18	0.13	0.05	0.04	0.09	0.07	<b>0.91</b>	<b>0.81</b>	<b>0.90</b>	0.75	0.89	0.74	<b>0.91</b>	<b>0.79</b>
Fog	0.14	0.11	0.20	0.17	0.20	0.17	<b>0.92</b>	<b>0.82</b>	<b>0.91</b>	<b>0.76</b>	0.87	0.72	0.84	0.69
Shadow	0.17	0.14	0.35	0.31	0.34	0.30	<b>0.94</b>	<b>0.84</b>	<b>0.94</b>	<b>0.82</b>	0.91	0.77	0.91	0.78
Occlusion	0.49	0.43	0.93	0.84	0.88	0.79	<b>0.97</b>	<b>0.90</b>	0.94	<b>0.84</b>	0.92	0.81	<b>0.95</b>	<b>0.84</b>
<b>Average</b>	0.23	0.19	0.43	0.38	0.49	0.42	0.82	0.67	0.83	0.65	<b>0.89</b>	<b>0.74</b>	<b>0.91</b>	<b>0.77</b>
<b>Minimum</b>	0.14	0.11	0.05	0.04	0.09	0.07	0.46	0.30	0.67	0.41	<b>0.87</b>	<b>0.68</b>	<b>0.85</b>	<b>0.67</b>

### B. Baselines

We compare the proposed TTA-Nav with six baselines: Pretrained-Nav, DD-PPO, TENT, SHOT-IM, DUA, and TENT-DUA. Among these baselines, TENT, SHOT-IM, DUA are task-agnostic and can be seamlessly integrated into our navigation model. Moreover, they have good performance in image recognition under domain shift and visual corruptions, the latter being a subset of domain shift. All baselines are evaluated with the same Gibson validation scenes used in [23]. Parameters of DD-PPO and Pretrained-Nav are frozen during testing, while others have adaptation.

- **Pretrained-Nav** is our navigation model that is fine-tuned from DD-PPO as explained in section III.
- **DD-PPO** [6] is the SOTA on a point-goal navigation task. See section III for more details.
- **DUA** [11] has the same model architecture as Pretrained-Nav, with the difference in that DUA updates the BatchNorm statistics  $\hat{\mu}_k$  and  $\hat{\sigma}_k$  during the test time with running mean and variance as explained in (2) and (3).
- **TENT** [12] is initialized with Pretrained-Nav’s architecture and parameters. Then, the model is fine-tuned with entropy loss during the test time. We follow the original

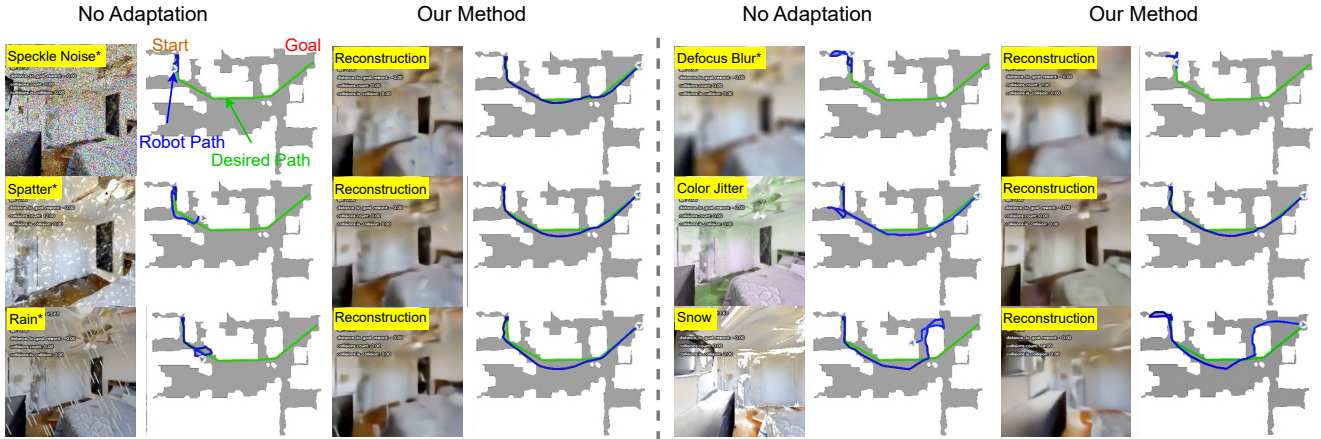


Fig. 5. **Navigation Behavior:** The figure shows examples of robot behavior in the same setting as used in Fig. 1. This navigation route is one of the most difficult routes in the scene ranked by the distance between start and goal. \* denotes the severe corruption<sup>1</sup>. *No Adaptation* refers to the non-adaptive state-of-the-art navigation model, DD-PPO. *Our Method* refers to TTA-Nav.

implementation of TENT by updating BatchNorm affine parameters but not updating other parameters.

- **TENT-DUA** closely resembles TENT, but differs primarily in its treatment of BatchNorm statistics update. While TENT-DUA employs moving average to update BatchNorm statistics, TENT does not use moving average. We expect this method to outperform TENT because it combines the advantages of both TENT and DUA.
- **SHOT-IM** [13] is initialized with the architecture and parameters of Pretrained-Nav. During the test time, the model undergoes fine-tuning using the Information Maximization (IM) loss. One of the two terms in IM loss is the same entropy loss as used in TENT. We fine-tune only  $\gamma$  and  $\beta$ , following the approach proposed by [12], as we find it enhances training stability. Additionally, BatchNorm statistics are updated with moving average during this process.

### C. Evaluation Metrics

**Success Rate (SR)** measures the proportion of success episodes among all evaluation episodes. An episode is deemed to be successful if an agent takes stop action within  $0.2m$  distance to a target position.

**Success weight by normalized inverse Path Length (SPL)** is proposed in [50]. We follow the same definition. Particularly,  $SPL = S \frac{l}{\max(l, p)}$ , where  $S$  is a binary indicator of success in an episode.  $l$  is the shortest path between the start and target of an episode, and  $p$  is the length of a path the agent takes.  $SPL$  is a strict metric in the sense that in order to achieve  $SPL = 1$  the agent must make no mistake, successfully arrive at the destination, and follow one of the shortest paths.

Regarding the last two rows of Table I, **Average** is the average of SR or SPL over all corruptions. **Minimum** is the minimum SR or SPL over all corruptions, delineating the lower bound of navigation performance.

TABLE II

**ABLATIONS:** THE TABLE SHOWS AVERAGE AND MINIMUM SR AND SPL OVER 14 SCENARIOS. SEE SUBSECTION IV-D FOR ANALYSIS.

	Average		Minimum	
	SR	SPL	SR	SPL
No Adapt	0.84	0.65	0.64	0.36
Block 1	0.90	0.75	0.81	0.63
Block 2	0.90	0.76	0.81	0.62
Block 3	0.89	0.75	0.78	0.60
All	<b>0.91</b>	<b>0.77</b>	<b>0.85</b>	<b>0.67</b>

### D. Results

**Adaptive Normalization implicitly does Image Restoration:** We compare reconstructions from test input images by TD with and without updating normalization parameters. Qualitatively, we can see in Fig. 4 that the reconstruction from adapted TD is brighter when input is dimmed and clearer when input is blurred or noisy. Color is changed to normal when the input image is dyed with yellow. Some water drops are removed by adapted TD. Moreover, if the input is clean, we can barely see the difference between the reconstructions of adapted and non-adapted TD.

**Navigation Under Visual Corruptions:** TTA-Nav shows remarkable improvement across all methods, achieving above 90% SR and above 78% SPL on the four most severe corruptions<sup>1</sup>. Additionally, TTA-Nav achieves the highest average SR and SPL across all types of visual observations. DUA is the second best-performing method, showing strong performance across multiple corruptions.

DUA’s performance decreases compared to its non-adaptive counterpart (Pretrained-Nav) when the visual observation is clean. In contrast, TTA-Nav maintains consistent performance levels akin to Pretrained-Nav under the no-corruption circumstance.

In real-world scenarios, it is imperative for a robot to

<sup>1</sup>As shown in Table I, *Speckle Noise*, *Lighting*, *Spatter*, *Rain*, and *Defocus Blur* can be classified as severe corruptions due to the substantial performance degradation observed in column 4, which is the SOTA navigation model (DD-PPO).

maintain a high SR under all circumstances. TTA-Nav is one of the best and closely comparable to the DUA in the minimum score regard. Generally, our TTA-Nav either ranks top 1 or 2. Its overall average performance is the best among all methods.

We also observe that TENT performs the worst among all the methods. A recent study [34] shows that TENT [12] has poorer performance compared to the same model without adaptation when the test data stream exhibits temporal correlation. The temporal correlation is a characteristic inherent in navigation images. Therefore, it is expected that TENT would struggle in this scenario. Moreover, SHOT-IM [13], which closely resembles TENT, also suffers from the temporal correlation.

**Ablations:** We study what layer with adaptation has the most effect on average and minimum SR and SPL scores. *No Adapt* refers to no update on normalization parameters, *Block 1,2* and *3* refer to update normalization parameters in VE’s block 1,2, and 3 respectively, while freezing the others. *All* refer to update all normalization parameters in the networks. By comparing rows 1 and 2 with row 3 in Table II, updating BatchNorm statistics in early layers seems to have the similar effect as our full model, while updating them on the later layer has less effect on boosting SR and SPL performances as indicated by the much lower minimum scores. This study suggests that updating BatchNorm statistics across all blocks is the best choice.

*Remark 1:* The main factor contributing to the improvement of navigation performance by TTA-Nav is adaptive normalization. It involves dynamically updating normalization statistics during the test phase. As illustrated in the first row of Table II, the model lacking adaptive normalization significantly underperforms compared to its adaptive counterpart. Additionally, adaptive normalization causes the emergence of image restoration within the VE without training on clean-corrupted pairs of images, as demonstrated earlier in Fig. 4.

*Remark 2:* The concept of image restoration emerging from adaptive normalization draws parallels with certain style transfer methods. Style transfer, which involves synthesizing a novel image by mixing the content of one image with the style of another, has been explored in [51], [52]. These studies demonstrate that  $\gamma$  and  $\beta$  in normalization layers represent styles, given that  $x$ ,  $\hat{\mu}$  and  $\hat{\sigma}$  correspond to content. See the definitions of these variables in (1). Essentially, the stylistic information is encapsulated within  $\gamma$  and  $\beta$ . Altering the style representation can be achieved by either training  $\gamma$  and  $\beta$  with a particular style [51] or setting them as style image statistics without training [52]. Regarding the parameters  $\gamma$  and  $\beta$  of our VE, they are pre-trained on “clean” images and remain fixed during testing. This suggests that they encapsulate the “style” of “clean” images. Meanwhile, our  $\hat{\mu}$  and  $\hat{\sigma}$  are recalculated at each environmental step via a moving average, signifying that they capture the content of the corrupted images. Consequently, given corrupted content images, our normalization layers facilitate the transfer of the style from the clean images to

generate cleaner reconstructed images.

## V. CONCLUSION

We present Test-time Adaptation (TTA) for point-goal navigation through our method TTA-Nav. Its key ideas are Top-down Decoder (TD) and adaptive normalization in the pre-trained navigation model. TD is integrated seamlessly with the pre-trained navigation model, offering robust adaptability to visually corrupted conditions without explicitly fine-tuning. TTA-Nav enhances navigation performance under visual corruptions without gradient-based optimization during the test time. Experimental results showcase TTA-Nav’s superior performance compared to SOTA TTA methods, including DUA [11], TENT [12], and SHOT-IM [13]. The results underscore its potential for widespread applications in robot navigation and other robotic tasks.

## ACKNOWLEDGEMENTS

The authors would like to acknowledge the assistance given by Research IT and the use of the Computational Shared Facility at The University of Manchester.

## REFERENCES

- [1] P. Chattopadhyay, J. Hoffman, R. Mottaghi, and A. Kembhavi, “Robustnav: Towards benchmarking robustness in embodied navigation,” in *Proceedings of the IEEE/CVF International Conference on Computer Vision*, 2021, pp. 15 691–15 700.
- [2] X. Zhao, H. Agrawal, D. Batra, and A. G. Schwing, “The surprising effectiveness of visual odometry techniques for embodied pointgoal navigation,” in *Proceedings of the IEEE/CVF International Conference on Computer Vision*, 2021, pp. 16 127–16 136.
- [3] F. Rajič, “Robustness of embodied point navigation agents,” in *European Conference on Computer Vision*. Springer, 2022, pp. 193–204.
- [4] R. Partsey, E. Wijmans, N. Yokoyama, O. Doboševych, D. Batra, and O. Maksymets, “Is mapping necessary for realistic pointgoal navigation?” in *Proceedings of the IEEE/CVF Conference on Computer Vision and Pattern Recognition*, 2022, pp. 17 232–17 241.
- [5] E. S. Lee, J. Kim, S. Park, and Y. M. Kim, “Moda: Map style transfer for self-supervised domain adaptation of embodied agents,” in *European Conference on Computer Vision*. Springer, 2022, pp. 338–354.
- [6] E. Wijmans, A. Kadian, A. Morcos, S. Lee, I. Essa, D. Parikh, M. Savva, and D. Batra, “Dd-ppo: Learning near-perfect pointgoal navigators from 2.5 billion frames,” in *International Conference on Learning Representations*, 2019.
- [7] J. Hu, L. Shen, and G. Sun, “Squeeze-and-excitation networks,” in *Proceedings of the IEEE conference on computer vision and pattern recognition*, 2018, pp. 7132–7141.
- [8] G. Kreiman and T. Serre, “Beyond the feedforward sweep: feedback computations in the visual cortex,” *Annals of the New York Academy of Sciences*, vol. 1464, no. 1, pp. 222–241, 2020.
- [9] H. Tang, M. Schrimpf, W. Lotter, C. Moerman, A. Paredes, J. Ortega Caro, W. Hardesty, D. Cox, and G. Kreiman, “Recurrent computations for visual pattern completion,” *Proceedings of the National Academy of Sciences*, vol. 115, no. 35, pp. 8835–8840, 2018.
- [10] M. Zhang, J. Feng, K. T. Ma, J. H. Lim, Q. Zhao, and G. Kreiman, “Finding any waldo with zero-shot invariant and efficient visual search,” *Nature communications*, vol. 9, no. 1, p. 3730, 2018.
- [11] M. J. Mirza, J. Micorek, H. Possegger, and H. Bischof, “The norm must go on: Dynamic unsupervised domain adaptation by normalization,” in *Proceedings of the IEEE/CVF Conference on Computer Vision and Pattern Recognition*, 2022, pp. 14 765–14 775.
- [12] D. Wang, E. Shelhamer, S. Liu, B. Olshausen, and T. Darrell, “Tent: Fully test-time adaptation by entropy minimization,” in *International Conference on Learning Representations*, 2020.
- [13] J. Liang, D. Hu, and J. Feng, “Do we really need to access the source data? source hypothesis transfer for unsupervised domain adaptation,” in *International conference on machine learning*. PMLR, 2020, pp. 6028–6039.

- [14] W. Burgard, A. B. Cremers, D. Fox, D. Hähnel, G. Lakemeyer, D. Schulz, W. Steiner, and S. Thrun, "The interactive museum tour-guide robot." in *Aaai/iaai*, 1998, pp. 11–18.
- [15] E. Marder-Eppstein, E. Berger, T. Foote, B. Gerkey, and K. Konolige, "The office marathon: Robust navigation in an indoor office environment," in *2010 IEEE international conference on robotics and automation*. IEEE, 2010, pp. 300–307.
- [16] A. J. Davison, I. D. Reid, N. D. Molton, and O. Stasse, "Monoslam: Real-time single camera slam," *IEEE transactions on pattern analysis and machine intelligence*, vol. 29, no. 6, pp. 1052–1067, 2007.
- [17] Y. Zhu, R. Mottaghi, E. Kolve, J. J. Lim, A. Gupta, L. Fei-Fei, and A. Farhadi, "Target-driven visual navigation in indoor scenes using deep reinforcement learning," in *2017 IEEE international conference on robotics and automation (ICRA)*. IEEE, 2017, pp. 3357–3364.
- [18] D. Pathak, P. Agrawal, A. A. Efros, and T. Darrell, "Curiosity-driven exploration by self-supervised prediction," in *International conference on machine learning*. PMLR, 2017, pp. 2778–2787.
- [19] Y. Ding, C. Florensa, P. Abbeel, and M. Phielipp, "Goal-conditioned imitation learning," *Advances in neural information processing systems*, vol. 32, 2019.
- [20] Manolis Savva\*, Abhishek Kadian\*, Oleksandr Maksymets\*, Y. Zhao, E. Wijmans, B. Jain, J. Straub, J. Liu, V. Koltun, J. Malik, D. Parikh, and D. Batra, "Habitat: A Platform for Embodied AI Research," in *Proceedings of the IEEE/CVF International Conference on Computer Vision (ICCV)*, 2019.
- [21] P. Marza, L. Matignon, O. Simonin, and C. Wolf, "Teaching agents how to map: Spatial reasoning for multi-object navigation," in *2022 IEEE/RSJ International Conference on Intelligent Robots and Systems (IROS)*. IEEE, 2022, pp. 1725–1732.
- [22] S. Chen, T. Chabal, I. Laptev, and C. Schmid, "Object goal navigation with recursive implicit maps," in *2023 IEEE/RSJ International Conference on Intelligent Robots and Systems (IROS)*. IEEE, 2023, pp. 7089–7096.
- [23] L. Mezghan, S. Sukhbaatar, T. Lavril, O. Maksymets, D. Batra, P. Bojanowski, and K. Alahari, "Memory-augmented reinforcement learning for image-goal navigation," in *2022 IEEE/RSJ International Conference on Intelligent Robots and Systems (IROS)*. IEEE, 2022, pp. 3316–3323.
- [24] D. Fried, R. Hu, V. Cirik, A. Rohrbach, J. Andreas, L.-P. Morency, T. Berg-Kirkpatrick, K. Saenko, D. Klein, and T. Darrell, "Speaker-follower models for vision-and-language navigation," *Advances in Neural Information Processing Systems*, vol. 31, 2018.
- [25] S. Raychaudhuri, T. Campari, U. Jain, M. Savva, and A. X. Chang, "Mopa: Modular object navigation with pointgoal agents," in *Proceedings of the IEEE/CVF Winter Conference on Applications of Computer Vision*, 2024, pp. 5763–5773.
- [26] J. Tobin, R. Fong, A. Ray, J. Schneider, W. Zaremba, and P. Abbeel, "Domain randomization for transferring deep neural networks from simulation to the real world," in *2017 IEEE/RSJ international conference on intelligent robots and systems (IROS)*. IEEE, 2017, pp. 23–30.
- [27] X. B. Peng, M. Andrychowicz, W. Zaremba, and P. Abbeel, "Sim-to-real transfer of robotic control with dynamics randomization," in *2018 IEEE international conference on robotics and automation (ICRA)*. IEEE, 2018, pp. 3803–3810.
- [28] Y. Ganin and V. Lempitsky, "Unsupervised domain adaptation by backpropagation," in *International conference on machine learning*. PMLR, 2015, pp. 1180–1189.
- [29] G. Kang, L. Jiang, Y. Yang, and A. G. Hauptmann, "Contrastive adaptation network for unsupervised domain adaptation," in *Proceedings of the IEEE/CVF conference on computer vision and pattern recognition*, 2019, pp. 4893–4902.
- [30] E. S. Lee, J. Kim, and Y. M. Kim, "Self-supervised domain adaptation for visual navigation with global map consistency," in *Proceedings of the IEEE/CVF winter conference on applications of computer vision*, 2022, pp. 1707–1716.
- [31] Y. Sun, X. Wang, Z. Liu, J. Miller, A. Efros, and M. Hardt, "Test-time training with self-supervision for generalization under distribution shifts," in *International conference on machine learning*. PMLR, 2020, pp. 9229–9248.
- [32] S. Goyal, M. Sun, A. Raghunathan, and J. Z. Kolter, "Test time adaptation via conjugate pseudo-labels," *Advances in Neural Information Processing Systems*, vol. 35, pp. 6204–6218, 2022.
- [33] W. Lin, M. J. Mirza, M. Kozinski, H. Possegger, H. Kuehne, and H. Bischof, "Video test-time adaptation for action recognition," in *Proceedings of the IEEE/CVF Conference on Computer Vision and Pattern Recognition*, 2023, pp. 22952–22961.
- [34] T. Gong, J. Jeong, T. Kim, Y. Kim, J. Shin, and S.-J. Lee, "Note: Robust continual test-time adaptation against temporal correlation," *Advances in Neural Information Processing Systems*, vol. 35, pp. 27253–27266, 2022.
- [35] W. Wang, Z. Zhong, W. Wang, X. Chen, C. Ling, B. Wang, and N. Sebe, "Dynamically instance-guided adaptation: A backward-free approach for test-time domain adaptive semantic segmentation," in *Proceedings of the IEEE/CVF Conference on Computer Vision and Pattern Recognition*, 2023, pp. 24090–24099.
- [36] L. Yuan, B. Xie, and S. Li, "Robust test-time adaptation in dynamic scenarios," in *Proceedings of the IEEE/CVF Conference on Computer Vision and Pattern Recognition*, 2023, pp. 15922–15932.
- [37] Y. Zhang, S. Borse, H. Cai, and F. Porikli, "Auxadapt: Stable and efficient test-time adaptation for temporally consistent video semantic segmentation," in *Proceedings of the IEEE/CVF Winter Conference on Applications of Computer Vision*, 2022, pp. 2339–2348.
- [38] Q. Wang, O. Fink, L. Van Gool, and D. Dai, "Continual test-time domain adaptation," in *Proceedings of the IEEE/CVF Conference on Computer Vision and Pattern Recognition*, 2022, pp. 7201–7211.
- [39] F. Xia, A. R. Zamir, Z.-Y. He, A. Sax, J. Malik, and S. Savarese, "Gibson Env: real-world perception for embodied agents," in *Computer Vision and Pattern Recognition (CVPR), 2018 IEEE Conference on*. IEEE, 2018.
- [40] A. Szot, A. Clegg, E. Undersander, E. Wijmans, Y. Zhao, J. Turner, N. Maestre, M. Mukadam, D. S. Chaplot, O. Maksymets, et al., "Habitat 2.0: Training home assistants to rearrange their habitat," *Advances in Neural Information Processing Systems*, vol. 34, pp. 251–266, 2021.
- [41] X. Puig, E. Undersander, A. Szot, M. D. Cote, T.-Y. Yang, R. Partsey, R. Desai, A. Clegg, M. Hlavac, S. Y. Min, et al., "Habitat 3.0: A co-habitat for humans, avatars, and robots," in *The Twelfth International Conference on Learning Representations*, 2023.
- [42] A. Chang, A. Dai, T. Funkhouser, M. Halber, M. Niessner, M. Savva, S. Song, A. Zeng, and Y. Zhang, "Matterport3d: Learning from rgb-d data in indoor environments," *arXiv preprint arXiv:1709.06158*, 2017.
- [43] S. Ioffe and C. Szegedy, "Batch normalization: Accelerating deep network training by reducing internal covariate shift," in *International conference on machine learning*. pmlr, 2015, pp. 448–456.
- [44] Y. Wu and K. He, "Group normalization," in *Proceedings of the European conference on computer vision (ECCV)*, 2018, pp. 3–19.
- [45] S. Hochreiter and J. Schmidhuber, "Long short-term memory," *Neural computation*, vol. 9, no. 8, pp. 1735–1780, 1997.
- [46] R. Child, "Very deep vae generalize autoregressive models and can outperform them on images," in *International Conference on Learning Representations*, 2020.
- [47] K. Pandey, A. Mukherjee, P. Rai, and A. Kumar, "Diffusevae: Efficient, controllable and high-fidelity generation from low-dimensional latents," *Transactions on Machine Learning Research*, 2022.
- [48] D. P. Kingma and J. Ba, "Adam: A method for stochastic optimization," *arXiv preprint arXiv:1412.6980*, 2014.
- [49] A. Buslaev, V. I. Iglovikov, E. Khvedchenya, A. Parinov, M. Druzhinin, and A. A. Kalinin, "Albumentations: fast and flexible image augmentations," *Information*, vol. 11, no. 2, p. 125, 2020.
- [50] P. Anderson, A. Chang, D. S. Chaplot, A. Dosovitskiy, S. Gupta, V. Koltun, J. Kosecka, J. Malik, R. Mottaghi, M. Savva, et al., "On evaluation of embodied navigation agents," *arXiv preprint arXiv:1807.06757*, 2018.
- [51] V. Dumoulin, J. Shlens, and M. Kudlur, "A learned representation for artistic style," *arXiv preprint arXiv:1610.07629*, 2016.
- [52] X. Huang and S. Belongie, "Arbitrary style transfer in real-time with adaptive instance normalization," in *Proceedings of the IEEE international conference on computer vision*, 2017, pp. 1501–1510.